PHYSICAL REVIEW C VOLUME 22, NUMBER 2 AUGUST 1980

Proton-proton bremsstrahlung at $T_p = 730$ MeV with photon energies up to 300 MeV

B. M. K. Nefkens, O. R. Sander,* and G. D. L. Webster
Department of Physics, University of California, Los Angeles, California 90024

D. I. Sober
Department of Physics, University of California, Los Angeles, California 90024
and Physics Department, The Catholic University of America, Washington, D.C. 20064 †

(Received 22 January 1980)

The results of new proton-proton bremsstrahlung differential cross section measurements at $T_p = 730$ MeV are presented. The experiment was designed to measure photons of 40-300 MeV at forward angles in coincidence with the scattered and recoil protons. The cross sections rise rapidly when $E_\gamma > 100$ MeV, in sharp disagreement with external-emission dominance calculations which predict a smooth and nearly flat spectrum. The model calculations of Tiator *et al.*, which consider the $\Delta(1232)$ resonance in the intermediate state, agree with our results, as does an adjusted soft-photon approximation calculation.

[NUCLEAR REACTIONS Proton-proton bremsstrahlung, $T = 730$ MeV; measured $\sigma(\theta, E_\gamma)$, 40–300 MeV; compared with soft-photon and isobar calculations.]

I. INTRODUCTION

Investigations of hadron-hadron bremsstrahlung may be divided into three groups:

(a) *Low energy studies,* at incident energies less than a few hundred MeV, where scattering is predominantly elastic. In this domain the measured differential bremsstrahlung cross sections agree, where tried, with the model-independent, parameter-free, soft-photon approximation (SPA) calculations based on the Low theorem.[1] This includes proton-proton,[2,3] neutron-proton,[2] and $\pi^\pm$-proton[4] bremsstrahlung. A simpler version of the SPA, known as EED,[5] also agrees very well with $\pi^\pm p$ bremsstrahlung data.[6]

(b) *High energy work,* at incident energies exceeding several GeV. No exclusive bremsstrahlung measurement has been reported in this region but there are experiments on inclusive production of high energy photons,[7,8] as well as on the related subject of lepton production.[8,9] A recent inclusive experiment on low energy, direct photon production[10] in $\pi^+ p$ interactions at 10 GeV/c shows good agreement with an SPA-type bremsstrahlung calculation.

(c) *Intermediate-energy interactions,* in the region between about 0.5 and 3 GeV incident energy where scattering is predominantly inelastic, and many resonances may be produced. The only exclusive experiment in this category, a proton-proton bremsstrahlung ($pp\gamma$) measurement at $T_p = 730$ MeV, was first reported[11] by us in 1977. We found[12] that the differential bremsstrahlung cross section for $E_\gamma < 100$ MeV agrees with SPA. However, when $E_\gamma > 100$ MeV the cross section increases rapidly and is much enhanced over SPA. One inclusive measurement[13] of the related process of direct positron production at $T_p = 800$ MeV has been reported. It yielded a zero result.

The enhancement of the $pp\gamma$ differential cross section for $E_\gamma > 100$ MeV at $T_p = 730$ MeV is the first clear deviation from SPA, and it has already generated an interesting variety of speculations as to its possible origin, including

(a) $\Delta(1232)$ resonance formation in the intermediate state,[14,15]

$$p + p \to p + \Delta^+ \to p + p + \gamma ,$$

(b) production of vector mesons in the intermediate state, e.g.,[16]

$$p + p \to p + p + \omega \to p + p + \gamma ,$$

(c) a very speculative possibility is the contribution to $pp\gamma$ from radiative transitions of six-quarks-in-a-bag states,

$$p + p \to (6q) \to (6q)' + \gamma \to p + p + \gamma$$

or

$$p + p \to (6q) \to p + p + \gamma .$$

To distinguish among these and other possibilities it is important to extend the $pp\gamma$ differential cross section measurements to photon energies above the limit of 205 MeV of Ref. 12. We have modified the apparatus used in Ref. 12 to extend the acceptance to $E_\gamma \simeq 300$ MeV. We report here on the new results obtained. The photon spectra increase sharply with increasing E_γ and are vastly different

from predictions based on external-emission dominance.

II. EXPERIMENTAL TECHNIQUE

The experiment was performed at the Lawrence Berkeley Laboratory 184 in. cyclotron, just prior to its retirement. The setup used is shown in Fig. 1. Much of the experimental apparatus, technique, and data analysis was identical to that of our previous $pp\gamma$ experiment,[12] hereafter referred to as Experiment I. Only the essential features of the experiment are outlined here, except where there are significant changes from Experiment I.

A proton beam of momentum 1380 ± 10 MeV/c ($T_p = 730 \pm 8$ MeV) was incident on a large, nearly flat, liquid hydrogen target which was inclined at an angle of $20.5° \pm 0.5°$ to the beam direction. All three final-state particles were detected. The momentum of one outgoing proton was measured by a wide-aperture magnetic spectrometer centered at 50.5° to the right of the beam line (looking downstream from the target). The protons thus detected will be referred to as "P_R." The spectrometer's angular acceptances were

$$44° < \alpha_R < 57°$$

horizontally and

$$-15° < \beta_R < 19°$$

vertically, where α is the clockwise (from above) angle in the horizontal plane away from the beam direction, and β is the vertical angle of elevation, measured upward from the horizontal plane. The subscript R denotes the right-side proton detector arm.

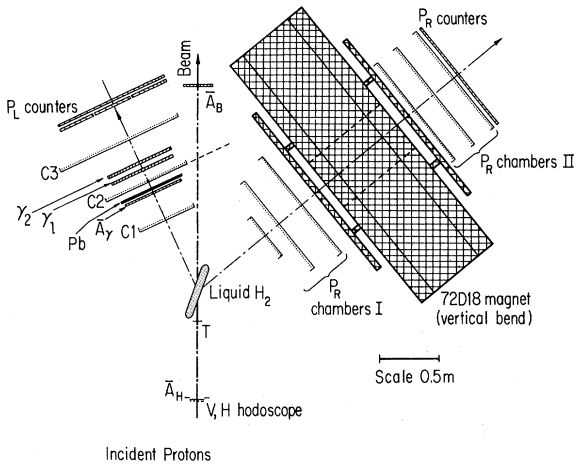

FIG. 1. Plan view of detection apparatus. $C1$–$C3$ are spark chambers; γ_1, γ_2, and A_γ are scintillation counters. Pb is a 1-cm-thick lead converter. The beam monitoring counters are described in Ref. 12.

The other outgoing proton, P_L, was detected on the left side of the beam by two spark chambers and two planes of scintillation counters in coincidence. This detector subtended the angles

$$-41° < \alpha_L < -9°$$

horizontally and

$$-16° < \beta_L < 0°$$

vertically, which corresponds to the lower half of the P_L detector of Exp. I. The P_L detector did not limit the horizontal acceptance of the experiment except for the highest photon energies, but did reduce the vertical acceptance to approximately half that of Exp. I.

For the purpose of detecting photons at angles very close to the P_L direction, we modified the P_L detector of Exp. I and used the upper half of chamber $C2$ from Exp. I as part of a new photon detector which is depicted in Figs. 1 and 2. This photon detector consisted of a 0.96-cm- (1.7 radiation lengths) thick lead sheet acting as a photon converter, followed by the spark chamber $C2$ and the plastic scintillation counters, γ_1 and γ_2. Only γ_1 was required in the event trigger. Preceding the lead converter was an anticounter, A_γ, for vetoing charged particles. To avoid complications in the readout of chambers $C2$ and $C3$ resulting from multiple sparks, we disabled the lower half of $C2$ and the upper half of $C3$, thereby reducing the ac-

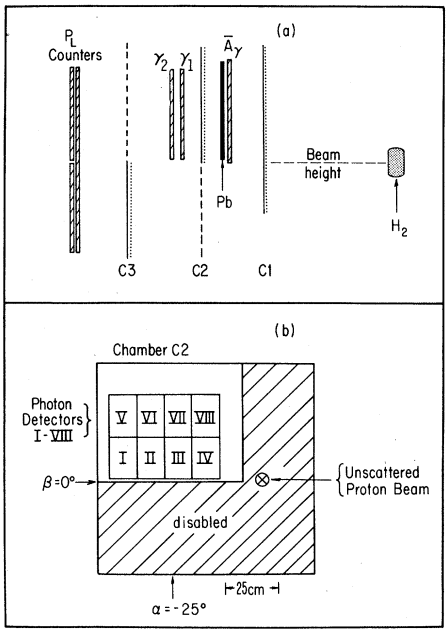

FIG. 2. Photon detection system. (a) Side view. (b) Front view of spark chamber $C2$, as seen from the target. The roman-numbered rectangles I–VIII are the "photon counters" G_{I}–G_{VIII} used in the analysis.

ceptance of P_L compared to Exp. I. The new photon detector subtended the angular range

$$-44° < \alpha_\gamma < -11°$$

horizontally and

$$0° < \beta_\gamma < 25°$$

vertically. For the analysis phase of the experiment this large detector was divided computationally into eight rectangular "photon counters," $G_{\rm I}$–$G_{\rm VIII}$, by binning all events according to the position of the photon in the $C2$ detector. The arrangement of the photon counters is shown in Fig. 2(b); the central positions of the counters are given in Table I.

In addition to these new photon detectors we used 15 of the original lead-glass photon detectors of Exp. I as alternative event triggers. They contributed about 35% of the total trigger rate and provided a measure of the overall efficiency. Elastic scattering runs for which the photon detectors were removed from the trigger were taken frequently to monitor the efficiency of the P_L detector. The two means of measuring efficiency were in very good agreement (within 5%).

III. DATA ANALYSIS

A. Event reconstruction

The procedure used in the data analysis was essentially the same as for Exp. I. Additional details can be found in Ref. 12.

For each event, we measured the directions of all incoming and outgoing particles as well as the momenta of the incident and right-scattered protons. The kinematics of the reaction was thus overdetermined by 2 degrees of freedom, allowing each recorded event to be subjected to a least-squares fitting routine in which a χ^2-like variable (henceforth referred to as "χ^2") was minimized. A small value for χ^2 indicates a high likelihood that the event is a true $pp\gamma$ event.

Those kinematic variables (including the photon energy E_γ) which were not directly measured were calculated from the best-fit variables for each event. The photon energy resolution Γ_γ therefore depended on the energy and angular resolutions of the entire detection system. In order to measure Γ_γ, elastic scattering ($pp \to pp$) events were analyzed as $pp\gamma$ events, with a fictitious photon directed toward each of the photon counters in turn. The width of the distribution of the (fictitious) E_γ thus obtained gives an empirical determination of Γ_γ for $pp\gamma$ events of very low E_γ. The resulting values of Γ_γ are given in Table II. The E_γ distributions of $pp \to pp$ events treated as $pp\gamma$ were centered on zero for all photon counters, indicating correct alignment of the apparatus.

A Monte Carlo simulation of $pp\gamma$ events with realistic measurement errors was used to calculate Γ_γ at various values of E_γ for each photon counter. The calculated widths at $E_\gamma = 0$ were some 30% smaller than the empirical values of Table II, but showed the same variation with photon counter.

In addition to $pp\gamma$ events, two principal types of background events were accepted by the trigger: (i) pp elastic scattering events in coincidence with a random trigger in a photon counter, and (ii) $pp \to pp\pi^0$ events with a gamma or random in the photon detector. Events of the first category had a uniform distribution in photon time of flight (TOF), and most were eliminated by imposing a TOF window of width 8 ns. Events outside the TOF window had an "E_γ" distribution centered at 0 and of width Γ_γ, in agreement with that for elastic scattering

TABLE I. Detector positions.

Detector	α (degrees)	β (degrees)	$d\Omega\gamma$ (msr)
$G_{\rm I}$	−39.5°	+6.5	30.4
$G_{\rm II}$	−31.5	+6.7	32.8
$G_{\rm III}$	−23.2	+6.7	33.4
$G_{\rm IV}$	−15.0	+6.6	32.0
$G_{\rm V}$	−39.5	+18.9	26.3
$G_{\rm VI}$	−31.5	+19.3	28.2
$G_{\rm VII}$	−23.2	+19.4	28.6
$G_{\rm VIII}$	−15.0	+19.2	27.5
P_R	44° to 57° [a]	−15° to +19° [a]	
P_L	−41° to −9°	−16° to 0°	

[a] For the approximation of our detector geometry by a point geometry, one should use the values $\alpha_R = 50.5°$ and $\beta_R = +9.2°$. The angles α and β are defined in the text.

TABLE II. Photon energy resolution in MeV (standard deviation) for each photon counter. 2nd column: experimentally determined resolution for $E_\gamma = 0$ MeV, obtained by treating pp elastic as $pp\gamma$ events; 3rd column: calculated resolution obtained from a sample of Monte Carlo generated events with $E_\gamma = 10$ MeV; 4th column: same as 3rd column but for $E_\gamma = 100$ MeV.

Photon counter	Exp $E_\gamma = 0$ MeV	M.C. $E_\gamma = 10$ MeV	M.C. $E_\gamma = 100$ MeV
I	10	7	7
II	15	9	9
III	20	12	10
IV	22	15	11
V	12	6	7
VI	12	8	9
VII	13	9	11
VIII	15	11	12

events. In order to prevent contamination of the $pp\gamma$ event sample by "random" events within the TOF window, we rejected all events whose reconstructed photon energy was less than 40 MeV for photon counters $G_{I,II}$ and $G_{V\text{-}VIII}$, and less than 60 MeV for G_{III} and G_{IV}. These E_γ cuts correspond to about $3\Gamma_\gamma$ from the elastic scattering peak at $E_\gamma = 0$.

Elimination of the $pp \to pp\pi^0$ background proved less difficult than one might fear. For the geometry of our detectors, there is a clean kinematic separation between $pp\gamma$ and $pp\pi^0$ except at the highest possible photon energies. For each photon counter, we can calculate an energy E_{clean} which is the minimum possible photon energy with which a $pp\pi^0$ event can be reconstructed as $pp\gamma$, including measurement errors. Thus, events with $E_\gamma < E_{clean}$ cannot be $pp\pi^0$. Values of E_{clean} for all photon counters are given in Table III.

For $E_\gamma > E_{clean}$, there exists the possibility that a $pp\pi^0$ event can simulate $pp\gamma$. To eliminate these events, we restrict the kinematics further by applying a cut described in Ref. 12, called the π^0 cut. This cut removes $pp\pi^0$ events while only slightly restricting the acceptance for $pp\gamma$ events, as described below.

The final discrimination of $pp\gamma$ from background events was made by means of a cut on the χ^2 value of each event. Figure 3 shows the χ^2 distribution of events in photon counter G_{IV} for three regions of E_γ. Each distribution shows a peak near $\chi^2 = 0$, which we associate with good $pp\gamma$ events. As in Exp. I, the shape of this peak agrees with Monte Carlo calculations which include measurement errors. A cut at $\chi^2 < 5$ was used in the final event selection. When $E_\gamma < E_{clean}$ (290 MeV for G_{IV}) the χ^2 distributions also show a small, slowly decreasing "tail" extending to high χ^2, which we associate with background events such as those involving doubly scattered protons. Such effects were not included in our Monte Carlo calculations. For $E_\gamma > E_{clean}$, a broad distribution at large χ^2 appears, agreeing in shape with our Monte Carlo calculations for $pp\pi^0$ events.

The effect of the π^0 cut may be clearly seen in Fig. 3. For $E_\gamma < E_{clean}$ the π^0 cut does not affect the χ^2 distribution, while for $E_\gamma > E_{clean}$ the π^0 cut removes the entire high-χ^2 "bump" but only reduces the $pp\gamma$ peak. The effect of the π^0 cut is taken into account when calculating the effective solid angle acceptance for $pp\gamma$, as described in

TABLE III. "Clean" photon energy (2nd column) and maximum possible photon energy (3rd column), as defined in the text, for each photon counter. The finite detector apertures and measurement errors were taken into account in obtaining these numbers.

Photon counter	E_{clean} (MeV)	$E_{\gamma(max)}$ (MeV)
I	190	260
II	230	290
III	270	205
IV	290	320
V	190	245
VI	210	270
VII	240	280
VIII	260	290

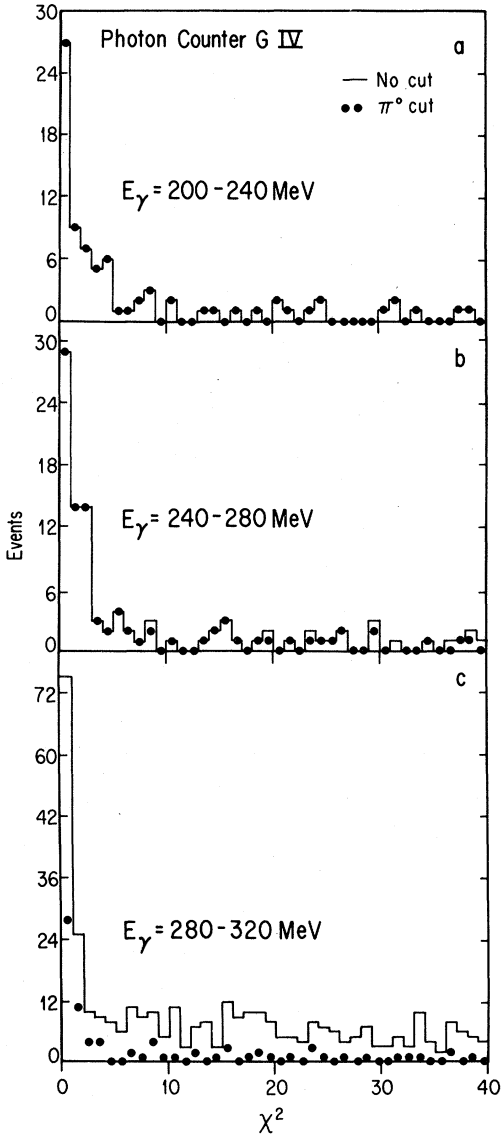

FIG. 3. χ^2 distribution of events recorded in photon counter G_{IV} and analyzed as $pp\gamma$ events for three intervals of reconstructed photon energy. The solid histogram represents the uncut data. The dots show the distribution after the π^0 cut has been applied.

Sec. III B.

The small background represented by the flat tail of the χ^2 distribution was assumed to extend under the $\chi^2 = 0$ peak, and a small subtraction, listed in Table IV, was made to eliminate such events. Another small subtraction was made to eliminate accidental coincidences within the 8 ns TOF acceptance region. The empty-target background was less than 1% of the number of good events, and no correction was necessary.

B. Cross section calculation

The experimental differential cross section in the laboratory system

$$\frac{d^3\sigma}{d\Omega_{PR} d\Omega_\gamma dE_\gamma} \tag{3.1}$$

was determined from the observed number of events (Table IV) as in Exp. I, with the following minor differences:

(a) The effective proton solid angle acceptance, $\Delta\Omega_{PR}$, was smaller. Since the P_L detector accepted only protons below the horizontal plane [see Fig. 2(a)], the effective aperture of the P_R detector, and therefore the proton solid angle acceptance, was reduced from its geometric value. At low E_γ, $\Delta\Omega_{PR} \simeq 72$ msr. At higher photon energies, the effect of the upward-going photon, which was usually associated with a downward-going P_L, increased the acceptance somewhat. This is more noticeable for the photon counters further above the horizontal plane (G_V–G_{VIII}). At the highest photon energies, certain angular ranges became kinematically impossible, reducing the acceptance ultimately to zero. The π^0 cut reduced the effective angular acceptance of the P_R detector at high energies. The effective proton solid angle acceptance, $\Delta\Omega_{PR}$, determined by Monte Carlo calculations, is shown for two photon counters in Fig. 4.

(b) The P_L chamber efficiency, ϵ_L, was lower, principally because the P_L proton was detected by only two spark chambers, in contrast to Exp I, where three chambers were used. Because of this lack of redundancy, ϵ_L could not be determined directly. Instead, the efficiency of the P_L chambers was monitored with frequent elastic scattering runs taken throughout the duration of the experiment. ϵ_L was determined from a comparison of these elastic scattering measurements with those of Exp. I, applying appropriate geometric cuts for the change in size of the P_L detector. The efficiency thus calculated did not vary from run to run; its average value is $49.2 \pm 1.3\%$, implying a reasonable individual chamber efficiency of 70%. An independent measurement of ϵ_L was made by a comparison of the numbers of events in the 15 lead-glass photon counters of this experiment and Exp. I with equal geometric cuts, yielding $\epsilon_L = 48.5 \pm 2\%$. The average detection efficiency for protons in the P_R chambers was 94.8%.

(c) Photon detection efficiency: The conversion of a photon into a detectable electron or positron was calculated using the results of two measurements[17,18] which spanned our range of photon energies. The resulting conversion efficiency function is shown in Fig. 5 together with the data points used in calculating it. The conversion efficiency varies from 0.34 at 40 MeV to 0.67 at 360 MeV, with an estimated error of less than ±0.04 over the energy region under consideration.[19]

(d) Photon spark chamber efficiency ϵ_γ: The efficiency of the photon detector spark chamber $C2$ was estimated from a study of correlations between the chamber and the two scintillator counters γ_1 and γ_2 located just behind it [Fig. 2(a)]. This yielded $\epsilon_\gamma = 85.4 \pm 1.0\%$.

IV. RESULTS

The differential cross sections in the laboratory system, $d^3\sigma/d\Omega_{PR} d\Omega_\gamma dE_\gamma$, for our eight photon counters are given in Table V as a function of the laboratory photon energy in 40 MeV bins. Because the cross section at low photon energy varies rapidly, roughly as $(E_\gamma)^{-1}$, we have limited the width

TABLE IV. Number of $pp\gamma$ events minus background.

Photon counter	Photon energy interval (MeV). 40–60	60–80	80–120	120–160	160–200	200–240	240–280	280–300
I	5	6–1	8	17–2	24–1	42–1	14[a]	
II	10–3	8–2	20–2	16–2	28–2	36–4	38–1	
III		19–5	35–4	40–4	49–4	56–4	76–7	25–1
IV		21–1	31–2	43–2	48–2	54–2	63–2	38–1
V	3	3	3	8	25	25		
VI	8–1	9	10	13	20	31	8[a]	
VII	10–4	16–2	25–2	31–2	41–2	33–2	32–1	
VIII	8–2	8	34–1	29–1	39–1	52–1	37–1	

[a] Photon energy interval limited to 240–260 MeV.

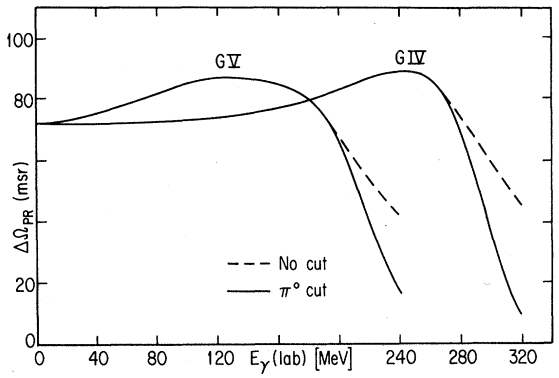

FIG. 4. Effective solid angle $\Delta\Omega_{PR}$ for detecting protons from $pp\gamma$ for events in photon counters G_{IV} and G_V.

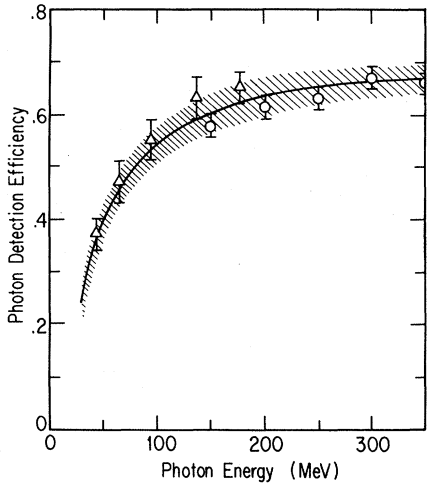

FIG. 5. Photon detection efficiency versus E_γ, for normal incidence on the 1.7-radiation-length converter, based on the data points of Refs. 17 (circles) and 18 (triangles). Spark chamber efficiency is not included. The solid curve shows the efficiency used, and the shaded area indicates its estimated error.

of the lowest two bins to 20 MeV. The errors are dominated by the statistical ones, except for the bins with $E_\gamma < 100$ MeV, where the uncertainty in the photon detection efficiency is large. Not included in the table is a systematic error of 15% due mainly to uncertainties in the detection efficiency and target thickness.

Our results are displayed in Fig. 6, where the lower scale indicates the photon energy in the laboratory system and the upper scale indicates the center of mass. The laboratory phase space factor increases rapidly when E_γ approaches its maximum possible value. Therefore, the rapid increase in the spectrum shown in Fig. 6 does not imply that the invariant bremsstrahlung matrix elements vary similarly rapidly.

To check on the stability of the data acquisition system throughout the experiment, we have divided our events into three subsamples according to the date of data taking. For each subsample we calculated the number of $pp\gamma$ events per 10^9 incident protons in two ranges of photon energy. The results for the three subsamples agree within statistics.

As discussed in Ref. 12, the set of five kinematic variables used to define the measured differential cross sections in the laboratory corresponds to two different kinematic configurations. As in Exp. I, the geometry of our apparatus renders it sensitive only to the so-called configuration I, the configuration with the larger value of θ_{PL}, as described in detail in Ref. 12. *Our quoted cross sections refer only to this configuration.*

V. DISCUSSION OF RESULTS

A. EED and SPA

The most straightforward calculations of $pp\gamma$ are those based on the soft-photon theorem of Low.[1] The two simplest versions, which we refer to as external-emission dominance[5,12] (EED) and soft-photon approximation[12] (SPA), are described briefly in the Appendix, where we also define the variables used in this section. EED gives a good

TABLE V. Laboratory differential cross sections $d^3\sigma/d\Omega_{PR}d\Omega_\gamma dE_\gamma$ in nb/sr^2 MeV for $pp \to pp\gamma$ at $T_p = 730$ MeV, for different photon energy intervals. Errors are statistical only; not included is a normalization uncertainty of 15%.

Photon counter	Photon energy interval (MeV) 40–60	60–80	80–120	120–160	160–200	200–240	240–280	280–300
I	8.1±5.1	5.1±3.0	3.2±1.3	5.1±1.6	7.5±1.9	18.1±3.9	27.5±9.0	
II	10.7±7.2	5.8±3.4	6.8±2.0	4.3±1.4	7.2±1.8	9.9±2.3	20.7±4.6	
III		13.3±5.4	11.6±2.8	11.5±2.5	12.8±2.6	13.7±2.6	22.0±4.3	37.5±9.7
IV		19.5±6.1	11.4±2.7	13.8±2.8	13.5±2.6	13.6±2.5	17.5±3.1	31.9±7.1
V	5.6±4.3	3.4±2.4	1.3±0.9	2.9±1.1	9.4±2.2	19.0±4.7		
VI	12.3±7.4	9.7±3.9	4.0±1.4	4.2±1.3	6.0±1.5	12.5±2.7	17.6±7.3	
VII	17±10	25.5±7.7	9.2±2.4	9.2±2.1	10.8±2.2	9.6±2.2	25.0±5.9	
VIII	10.7±7.3	8.7±3.7	13.7±3.1	9.3±2.1	10.8±2.2	15.4±2.8	17.7±3.9	

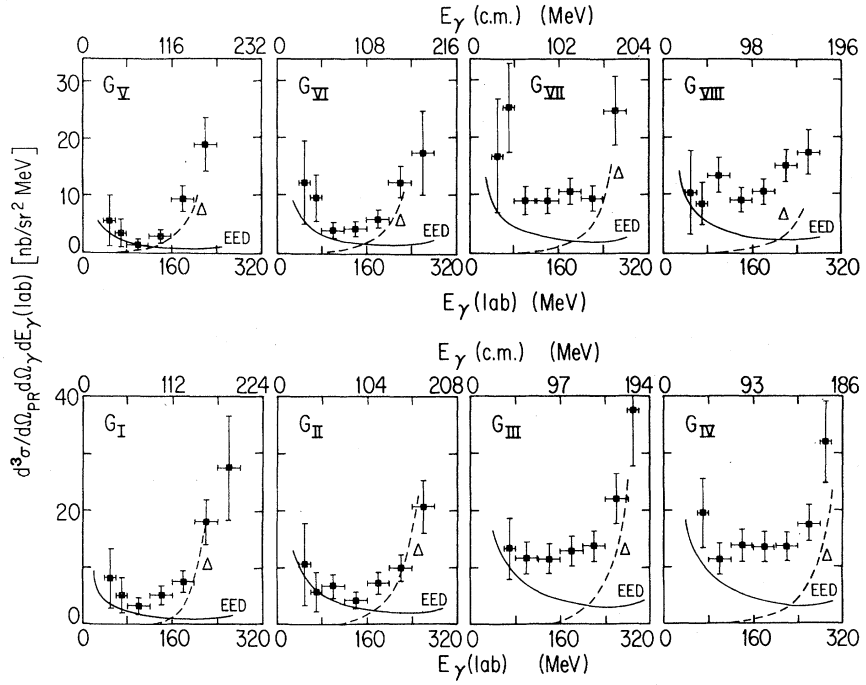

FIG. 6. Differential cross sections in the laboratory system vs photon energy in the laboratory (lower scale) and center of mass (upper scale). The horizontal bars indicate the width of each photon energy bin. The solid curve is the EED($\bar{s},\bar{t}$) calculation, averaged by Monte Carlo method over the acceptance of the detectors. The dashed line shows the Δ isobar contribution calculated by Tiator *et al.* (Refs. 14 and 21).

account of the data of Exp. I up to photon energies of at least 60 MeV, but falls progressively farther below the cross sections as E_γ increases.

We have carried out EED calculations for the present experiment. Elastic cross sections were taken from the experimental fits of Ryan *et al.*[20] The effects of our finite detector sizes were calculated by averaging the cross section over the experimental acceptance using a Monte Carlo program, a procedure made very inexpensive by the simple form of the EED cross section. In all our calculations for Exp. I, we used the "standard" choice of variables $\bar{s},\bar{t}$, as defined in the Appendix Whenever this is the case in the subsequent discussion and accompanying figures, we shall use the notation EED($\bar{s},\bar{t}$) to denote this choice.

It is instructive to examine the magnitude of the uncertainty in EED introduced by the ambiguity in the choice of s and t under the conditions of this experiment. The ranges of s and t are given by $s_f < s < s_i$ and $|t_1| < |t| < |t_2|$. (The symbols are defined in the Appendix.) One approach frequently used in SPA calculations is to use a different value of s,t for each of the four external-emission Feynman amplitudes. Applying this technique here would violate the spirit of the EED calculation. We choose instead to preserve the simplicity of the EED result, in which the $pp\gamma$ cross section is proportional to the elastic cross section, and limit ourselves to the question of the allowable variation of the s,t values at which a single elastic cross section $(d\sigma/d\Omega)(s,t)$ is evaluated.

In Fig. 7 we show for photon counters G_{IV} and G_{VII} the results of the following variations:

(1) EED($\bar{s},\bar{t}$)—the "conventional" choice,

(2) EED(s_0,t_0)—the s and t of an elastic scattering event with the same laboratory angle as the P_R

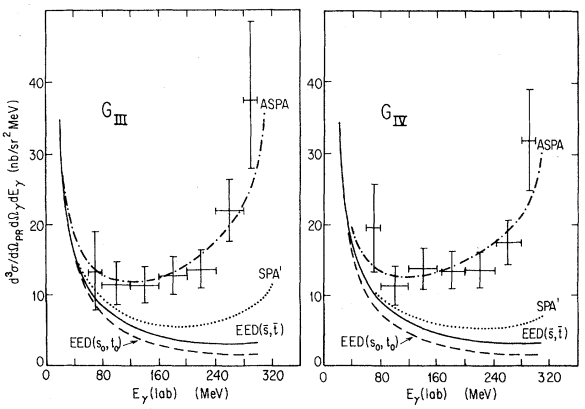

FIG. 7. Laboratory differential cross section for two photon counters, compared with various soft-photon calculations as described in the text.

proton.

In Exp. I, the full SPA calculations of Fearing,[12] which agreed with the data up to $E_\gamma \simeq 100$ MeV, were based on an expansion about $\bar{s}, \bar{t}$. A complete SPA calculation for the present geometry is not yet available.

In the meantime, the detailed SPA calculations presented in Ref. 12 allow us to draw the following conclusions (see Fig. 11 of Ref. 12):

(a) The interference term $2\mathrm{Re}(AB^*)/k$ at $T_p = 730$ MeV at all measured photon energies and angles is less than 10% of the sum of the first and second terms $(A^2/k^2 + B^2)$, and can be neglected. (k is the photon momentum in the center of mass system.) The same appears to be true at other incident proton energies as well.[3]

(b) The B^2 term does not vary appreciably with photon energy or angle. Note that we refer here to the squares of the invariant amplitudes and *not* to the cross sections (which include the phase space factor).

In the absence of a full SPA calculation we have constructed two approximations to SPA:

(1) SPA′, which consists of EED plus a constant B^2 term of magnitude 3.4×10^4, a reasonable value suggested by the outcome of the SPA calculations of Ref. 12 (where the normalization of the invariant matrix element is defined). The SPA′ results are compared with our data in Fig. 7. The agreement is good up to $E_\gamma \simeq 100$ MeV. At higher photon energies SPA′ is substantially smaller than our data.

(2) Adjusted soft-photon approximation (ASPA), which consists of EED plus a B^2 term which is constant for each photon counter. The ASPA results are compared with some of our data in Fig. 7. The values of B^2 used are 1.9×10^5 for G_{III} and 2.3×10^5 for G_{IV}. The agreement is good up to the highest photon energy for all photon counters, implying that the $pp\gamma$ differential cross section as function of E_γ can be described adequately up to the highest measured photon energy, $E_\gamma = 300$ MeV, by a simple power series expansion in the photon momentum k, with the highest power being of order k. (See also Sec. V C of Ref. 12 for a similar suggestion.)

B. Isobar excitation models

Tiator, Weber, and Drechsel[14] have evaluated the contribution of the radiative decay of the $\Delta(1232)$ isobar to $pp\gamma$. The calculation is Lorentz and gauge invariant, and uses conventional coupling constants and form factors. The final $pp\gamma$ cross section is taken to be the incoherent sum of EED and the radiative isobar decay contribution. The numerical results for point geometry, i.e., using the centers of the detectors to define the angles, have been evaluated by Tiator.[21] The calculated Δ contribution is shown in Fig. 6 together with our data. The theory accounts remarkably well for the steep rise in the spectrum observed experimentally at high E_γ. Although the Tiator predictions have not yet been averaged over the finite size of the detectors, such geometric corrections for our apparatus are typically less than 20%. We conclude that the model of Tiator *et al.* is in agreement with our data.

Szyjewicz and Kamal[15] have made a field theoretical $pp\gamma$ calculation in which the external-emission diagrams are evaluated in a one-boson exchange model. Good agreement is obtained with measurements at $T_p = 200$ MeV. However, at 730 MeV the calculations at small E_γ do not approach the EED values, presumably because no form factors were used. The shape of our 730 MeV data is reasonably well reproduced after inclusion of the Δ excitation, which causes the cross section at high E_γ to increase with increasing E_γ, as in the model of Tiator *et al.* Numerical predictions for our new geometry are not available as yet but the qualitative features are those discussed in Ref. 12.

C. Other models

An interesting alternative to the Δ-excitation model discussed in the previous section is bremsstrahlung via a vector meson intermediate state.[16,22] At $T_p = 730$ MeV the shape of the photon spectrum is qualitatively that found in this experiment and not substantially different from those obtained in the Δ-excitation model. A possible way to distinguish the two mechanisms is a measurement of the $pp\gamma$ photon spectrum at a higher incident energy, say $T_p = 1$ GeV, or for smaller-angle proton scattering. At the proper geometrical configuration,[21] the Δ-excitation mechanism leads to a clear bump in the photon spectrum, with the position of the bump determined by the mass of the Δ. (We note, however, that similar predictions for the contribution to $\pi^+p \to \pi^+p$ were not verified experimentally.[6]) In contrast, the vector meson model will lead to a photon spectrum which peaks at a much higher energy.

A completely different mechanism for an enhancement of $pp\gamma$ is the radiative decay of possible six-quarks-in-a-bag states Q. When the incident proton energy is appropriate to produce a Q, the latter can decay to a lower-lying Q state with emission of a monochromatic photon which should be a unique signature for identifying Q states. A Q state can also decay radiatively, $Q \to pp\gamma$. The masses and quantum numbers of Q states have been estimated recently by Wong and Liu,[23] and have the right values to give a possible contribution to our measurement.

VII. CONCLUSIONS

The new measurements of the differential cross section for proton-proton bremsstrahlung at $T_p = 730$ MeV for forward-going photons show a cross section which increases steeply with photon energy above $E_\gamma \simeq 100$ MeV, in contrast with the EED and SPA calculations. The shape of the photon spectrum agrees with the Δ-excitation model calculation of Tiator *et al.*, and with an "adjusted soft-photon calculation" which includes an arbitrary term of order k. It appears that $pp\gamma$ in the intermediate-energy region provides the most exciting deviation from soft-photon calculations yet seen in radiative process.

ACKNOWLEDGMENT

This work was supported by the U. S. Department of Energy. Part of the work of one of the authors (D.I.S.) was supported by the National Science Foundation. We gratefully acknowledge the hospitality extended to us at the Lawrence Berkeley Laboratory and the dedicated help of the personnel of the 184 in. cyclotron. Nancy Matz and Bill Plumlee provided important assistance in data taking. David Smith was helpful in adapting the computer reconstruction programs. Mike O'Neill did much of the computer analysis work. We thank Harold Fearing and Leon Heller for useful discussions.

APPENDIX: THE SOFT-PHOTON APPROXIMATION

The bremsstrahlung matrix element may be expanded in a power series in the photon momentum k:

$$M = A/k + B + Ck + \cdots . \tag{A1}$$

The bremsstrahlung cross section is then

$$\begin{aligned} d\sigma &= |M|^2 \phi \sim |M|^2 k \\ &= A^2/k + 2\,\mathrm{Re}(AB^*) + B^2 k + 2\,\mathrm{Re}(AC^*)k \\ &\quad + 2\,\mathrm{Re}(BC^*)k^2 + C^2 k^3 \\ &\quad + (\text{other terms of order } k^2 \text{ and higher}) . \end{aligned} \tag{A2}$$

ϕ is a normalized phase space factor which is approximately proportional to k.

Low[1] first showed that in the soft-photon limit, $k \to 0$, the coefficients A and B of Eq. (A1) can be determined from the on-shell elastic scattering amplitudes. Thus, the first three terms of Eq. (A2) are calculable in a model-independent way. The soft-photon approximation (SPA) is the procedure for calculating the A and B terms based on Low's prescription when $k \neq 0$. The necessary elastic scattering amplitudes are now off the mass shell. As these amplitudes are in general unknown, they are approximated by nearby on-shell amplitudes. The extrapolation of elastic amplitudes off the mass shell is *not* an unambiguous procedure, and thus there can be several different approximations leading to different "realizations" of the SPA, differing in terms of order k.[24]

The laborious calculation of the A and B terms by the Low prescription can be greatly simplified by applying a spin summation theorem due to Burnett and Kroll.[25] This makes it possible to write the first term of the bremsstrahlung cross section, Eq. (A2), as the product of the elastic scattering *cross section* multiplied by kinematic factors of order $1/k$. External-emission dominance[5] (EED) is the name given to the approximation of the bremsstrahlung cross section by the first term of Eq. (A2) calculated in this particular way. The EED calculation requires only experimentally determined elastic scattering cross sections as input. In contrast, the calculation of the B^2 term of Eq. (A2) requires a parametrization of the elastic scattering amplitudes.

Conservation of energy and momentum for $pp \to pp\gamma$ implies

$$P_1 + P_2 = P_3 + P_4 + K . \tag{A3}$$

The capital letters represent the four-vector momenta of the initial-state (P_1, P_2) and final-state (P_3, P_4) protons and of the photon (K). The squares of the hadronic total energy in the initial and final states are

$$\begin{aligned} s_i &= (P_1 + P_2)^2 , \\ s_f &= (P_3 + P_4)^2 . \end{aligned} \tag{A4}$$

The squares of the four-momentum transfers are

$$\begin{aligned} t_1 &= (P_1 - P_3)^2 , \\ t_2 &= (P_2 - P_4)^2 . \end{aligned} \tag{A5}$$

In the soft-photon limit, the kinematics of the bremsstrahlung reaction reduces to those of elastic scattering:

$$\begin{aligned} s_i(\text{elastic}) &= s_f(\text{elastic}) \equiv s_0 , \\ t_1(\text{elastic}) &= t_2(\text{elastic}) \equiv t_0 . \end{aligned} \tag{A6}$$

A common choice of on-shell kinematics at which to evaluate s and t in SPA calculations is

$$\begin{aligned} \bar{s} &= (s_i + s_f)/2 , \\ \bar{t} &= (t_1 + t_2)/2 . \end{aligned} \tag{A7}$$

*Present address: Los Alamos Scientific Laboratory, Los Alamos, New Mexico 87545.
†Present address.

[1]F. Low, Phys. Rev. 110, 974 (1958).
[2]E. M. Nyman, Phys. Rev. 170, 1628 (1968).
[3]H. W. Fearing, in *Nucleon-Nucleon Interactions*, Proceedings of the Second International Conference on Nucleon-Nucleon Interactions, Vancouver, 1977, edited by Harold Fearing, David Measday, and Ada Strathdee (AIP, New York, 1978).
[4]M. K. Liou and W. T. Nutt, Phys. Rev. D 16, 2176 (1977).
[5]B. M. K. Nefkens and D. I. Sober, Phys. Rev. D 14, 2434 (1976).
[6]B. M. K. Nefkens, M. Arman, H. C. Ballagh, P. F. Glodis, R. P. Haddock, K. C. Leung, D. E. A. Smith, and D. I. Sober, Phys. Rev. D 18, 3911 (1978).
[7]P. Darriulat *et al.*, Nucl. Phys. B110, 365 (1976).
[8]J. H. Cobb *et al.*, Phys. Lett. 78B, 519 (1978).
[9]E. W. Beier *et al.*, Phys. Rev. Lett. 37, 1117 (1976).
[10]A. T. Goshaw *et al.*, Phys. Rev. Lett. 43, 1065 (1979).
[11]B. M. K. Nefkens, O. R. Sander, and D. I. Sober, Phys. Rev. Lett. 38, 876 (1977).
[12]B. M. K. Nefkens, O. R. Sander, D. I. Sober, and H. W. Fearing, Phys. Rev. C 19, 877 (1979).
[13]A. Browman *et al.*, Phys. Rev. Lett. 37, 246 (1976).
[14]L. Tiator, H. J. Weber, and D. Drechsel, Nucl. Phys. A306, 468 (1978).
[15]A. Szyjewicz and A. N. Kamal, in *Few Body Systems and Nuclear Forces*, proceedings of the VIII International Conference on Few Body Systems and Nuclear Forces, Graz, Austria, 1978, edited by H. Zingl, M. Haftel, and H. Zenkel (Springer, Berlin, 1978), Vol. 82, p. 88.
[16]A. N. Kamal and A. Szyjewicz, Nucl. Phys. A285, 397 (1977).
[17]D. I. Sober, R. P. Haddock, B. M. K. Nefkens, and B. L. Schrock, Nucl. Instrum. Methods 109, 29 (1973).
[18]P. Darriulat, E. Gygi, M. Holder, K. T. McDonald, H. G. Pugh, F. Schneider, and K. Tittel, Nucl. Instrum. Methods 129, 105 (1973).
[19]For a discussion of the consistency of these conversion measurements, see D. I. Sober, Nucl. Instrum. Methods 166, 555 (1979).
[20]B. A. Ryan, A. Kanofsky, T. J. Devlin, R. E. Mischke, and P. F. Shepard, Phys. Rev. D 3, 1 (1971).
[21]L. Tiator, private communication.
[22]R. Rückl, private communication.
[23]C. W. Wong and K. F. Liu, Phys. Rev. Lett. 41, 82 (1978).
[24]A lucid discussion of this point is given by L. Heller, in *Few Body Systems and Nuclear Forces*, proceedings of the VIII International Conference on Few Body Systems and Nuclear Forces, Graz, Austria, 1978, edited by H. Zingl, M. Haftel, and H. Zenkel (Springer, Berlin, 1978).
[25]T. H. Burnett and N. M. Kroll, Phys. Rev. Lett. 20, 86 (1968).